Aerosol and Air Quality Research, 17: 1489–1500, 2017

ISSN: 1680-8584 print / 2071-1409 online
doi: 10.4209/aaqr.2016.10.0443

Analysis of a Multi-Year Record of Size-Resolved Hygroscopicity Measurements from a Rural Site in the U.S.

Manasi Mahish, Don Collins*

Department of Atmospheric Sciences, Texas A&M University, College Station, Texas 77843-3150, USA

ABSTRACT

Hygroscopic growth factor (GF) distributions of 13, 25, 50, 100, 200, and 400 nm particles measured with a Hygroscopic Tandem Differential Mobility Analyzer (HTDMA) from 2009 to 2012 at the Southern Great Plains (SGP) site in Oklahoma, U.S. were used to describe time of day- and annually-averaged hygroscopicity parameters (κ). A diel pattern was often observed with an average daytime κ that was higher than that at other times, especially on days with new particle formation (NPF) events. The average hygroscopicity of the smaller and larger particles at the tails of the measured size range was higher than that in between, with the minimum for each of the 4 years at 50 nm. This pattern is thought to result in part from addition of soluble inorganic and organic compounds formed through gas phase and aqueous phase reactions for the smaller and larger particles, respectively. The size dependence is reflected in the averaged κ and in the frequency with which GF distributions possessed modes categorized as nearly-hydrophobic, less hygroscopic, and hygroscopic. A hygroscopicity-based mixing state parameter, MS_{hyg}, defined as the ratio of the standard deviation (SD) of a measured GF distribution to the size specific threshold SD roughly separating internal and external mixtures, was used to study the diel and seasonal variation in particle mixing state. Internal mixtures were found to be more common during the daytime and during the summer, likely reflecting more rapid photochemical processing and growth at those times.

Keywords: Aerosol; Hygroscopicity; Growth factor; Mixing state.

INTRODUCTION

Atmospheric particles influence climate by scattering and absorbing solar radiation and by acting as cloud condensation nuclei (CCN). The extent of their influence depends on the size of the particles, which can be significantly increased for hygroscopic aerosols when exposed to high relative humidity (RH). Among common atmospheric particle types, those composed of soluble inorganic species are generally the most hygroscopic, while those composed of organics exhibit a range in hygroscopicity with some being slightly hygroscopic (Svenningsson *et al.*, 2006; Prenni *et al.*, 2007; Duplissy *et al.*, 2008; Gunthe *et al.*, 2009; Jurányi *et al.*, 2009; King *et al.*, 2010; Yli-Juuti *et al.*, 2011) and others non-hygroscopic (Abbatt *et al.*, 2005; Prenni *et al.*, 2007). Major inorganic species such as ammonium, sulfate, nitrate, and chloride are typically the primary contributors to water uptake and consequent hygroscopic growth of atmospheric aerosols. The varied and complex composition of organic aerosols results in varied hygroscopicity that remains an active area of study. Organics can also influence water uptake by inorganic species in the same particle, with studies showing decreased water uptake by inorganic salts above their deliquescence RH (DRH) and increased uptake below it relative to particles composed of the pure species (Dick *et al.*, 2000; Hersey *et al.*, 2009; Meyer *et al.*, 2009). Other studies have shown that the influence of organics differs among inorganics, with addition of commonly found organics resulting in decreased water uptake by NaCl but increased water uptake by $(NH_4)_2SO_4$ (Cruz *et al.*, 2000; Choi *et al.*, 2002). The effect of organics on the hygroscopicity of multi-component aerosols varies by type and amount, but often can be explained by the simple ZSR mixing rule at RH above the DRH (Jing *et al.*, 2016; Peng *et al.*, 2016). This link with composition supports the use of hygroscopicity as a rough proxy for particle type (McMurry and Stolzenburg, 1989; Zhang *et al.*, 1993; Gysel *et al.*, 2007), with higher growth indicating a higher soluble inorganic content and lower growth indicating a higher content of organics and/or insoluble components such as soot and dust.

Hygroscopic growth of an aerosol is often measured using a Hygroscopic Tandem Differential Mobility Analyzer (HTDMA), which was first illustrated by Liu *et al.* (1978). The measured distribution of particle hygroscopicity is usually reported in terms of the hygroscopic growth factor or simply Growth Factor (GF), which is the ratio of the

* Corresponding author.
Tel.: 1-(979) 862-4401; Fax: 1-(979) 862-4466
E-mail address: dcollins@tamu.edu

diameter of a particle (D) at high relative humidity to its dry size ($D_{high\ RH}/D_{dry}$). Gasparini *et al.* (2006) reported increased hygroscopicity with increasing particle size based on HTDMA measurements made in May 2003 at the Department of Energy's (DOE) Southern Great Plains (SGP) Atmospheric Radiation Measurement (ARM) site in an agricultural area of Oklahoma, U.S., which is also where the data reported here were collected. This result is consistent with the findings of Holmgren *et al.* (2014), Levin *et al.* (2014), and others. An interpretation of this size dependent hygroscopicity is a higher organic content in smaller particles. Levin *et al.* (2014) reported results from an elevation of 2300 m in Pike National Forest in the central Rocky Mountains of Colorado, U.S. Their study support this interpretation, with higher organic fraction in smaller particles and increasing inorganic fraction in larger particles.

Aerosol hygroscopicity in continental locations often exhibits a diel pattern, frequently being higher during the day and lower at night, as observed in a boreal forest in Hyytiälä, southern Finland (Ehn *et al.*, 2007), and at a polluted site of the North China Plain (Liu *et al.*, 2011). The relatively unpolluted boreal forest in Hyytiälä offers an assessment of the characteristics of aerosols derived primarily from biogenic precursor emissions. In contrast, the highly polluted site at the North China Plain is surrounded by an area with mixed agricultural, residential, and industrial land use, and thus exhibits significant influence from anthropogenic sources. The pattern at Hyytiälä has been attributed to higher gas phase concentration of sulfuric acid during the day (Fiedler *et al.*, 2005), and abundant less hygroscopic organic compounds at night (Sellegri *et al.*, 2005). The diel pattern observed at the North China Plain has been attributed to accumulation of freshly emitted non-hygroscopic particles near the surface at night and of aged particles during the day. Holmgren *et al.* (2014), however, found more hygroscopic aerosols at night than during the day at the high altitude site, Puy de Dôme, France, where boundary layer dynamics and long range transport play more important roles.

Holmgren *et al.* (2014) used hygroscopicity data to derive growth factor probability density functions (GF-PDFs) and used them to quantify aerosol mixing state. They described aerosols for which GF-PDFs had standard deviations (SD) less than 0.1 as internal mixtures and those with SD higher than 0.15 as external mixtures. For external mixtures, at least two modes were identified. The median GF and number concentration of each mode were determined and the mode was then categorized into one of three groups: more-hygroscopic, hygroscopic, or less-hygroscopic. Their study explored the influences of particle size and seasons on mixing state. They found that accumulation mode particles were more frequently in external mixtures during autumn and winter.

Our study uses size and GF distributions to analyze the overall hygroscopic properties of the aerosol population, the variation of those properties seasonally, with time of day, and with particle size, and the connection of those properties and their time dependence with new particle formation (NPF) events. Additionally, the mixing state of the aerosol has been quantified using a particle size dependent threshold SD (i.e., SD(D)) over the full measurement size range.

SITE DESCRIPTION

The submicron size distributions and size-resolved hygroscopic growth distributions were measured at SGP (36°36'19.6"N, 97°29'20.7"W, 315 m above sea level) between 2009 and 2012. Although this site is primarily a mixed land use area of cattle pastures and agricultural fields, transported air masses from other regions bring diversity in aerosol concentration and properties. The wind rose diagram for nearby Ponca City (Fig. 1) shows that winds at the site are most frequently from the south and southeast and less frequently from the north. Parworth *et al.* (2015) described the seasonal distribution of air mass transport in 2011–2012 based on the NOAA HYSPLIT model. During the summer, winds were most often from the south and southeast, while during the winter they were largely from the north. Winds in the spring and fall were more variable. Air from local and surrounding agricultural fields carries secondary organic aerosol (SOA) and high concentrations of gas phase bases. Air arriving from the south often has elevated sulfur dioxide (SO_2) originating from electricity production, industrial facilities, and fuel combustion, and nitrogen oxides ($NO_x = NO + NO_2$) from industrial facilities and vehicle emissions. Air arriving from the north commonly brings SOA precursors (Hodshire *et al*., 2016), and lower (than with southerly winds) concentrations of NO_x. The county-wise emission densities of SO_2 and NO_x are shown in Tables S1–S2, and Fig. S1 to elucidate their relative contributions from different directions. The site is far enough downwind of most major anthropogenic sources that the aerosol is diluted during transport (Parworth *et al*., 2015).

INSTRUMENT DETAILS

The SMPS/HTDMA system that produced the data used in this analysis was fabricated at Texas A&M University and housed in the Aerosol Observing System (AOS) trailer, which is one of the many permanent trailers at SGP. The instrument is maintained by DOE ARM and all data reported here were taken directly from the open access data archive at http://www.archive.arm.gov. Details of the instrument and data processing are described in an instrument handbook also available through the archive website (Collins, 2010) and will only be briefly summarized here. The system sequentially measures a size distribution while operating as an SMPS and then a set of size-resolved hygroscopic growth factor distributions at 90% RH while operating as an HTDMA. The sampled aerosol enters the AOS trailer through a ~10 m high inlet and is dried to below 20% RH with a Nafion tube bundle. A Po-210 neutralizer is used to bring the aerosol to a steady state charge distribution. The sheath and sample flow rates are maintained at a ratio of 10:1 and are maximized for each size or hygroscopic growth factor measurement with the constraints that the high voltage not exceed the threshold for arcing and the sample flow rate not exceed ~95% of the 3 L min^{-1} flow rate of the

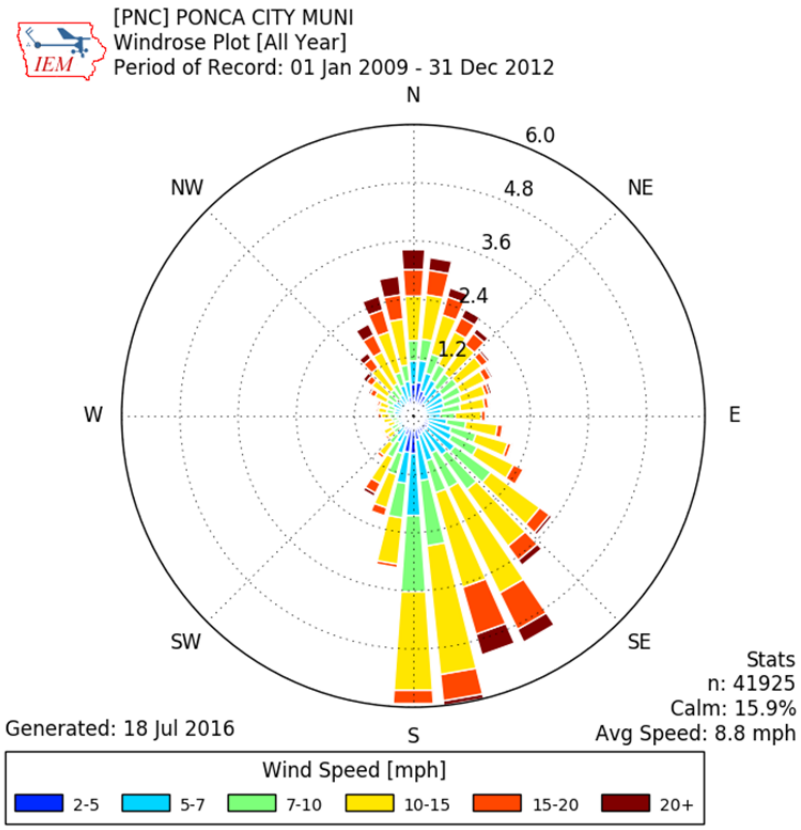

Fig. 1. Wind rose plot for Ponca City, OK, for 2009–2012. (Source: http://mesonet.agron.iastate.edu).

TSI 3762 CPC. A pair of high flow DMAs (Stolzenburg *et al*., 1998) are used to maximize sample flow rate and, with it, particle count rate and statistics. Size distributions spanning a diameter range of 12 to 750 nm are measured with a scan time of 150 s and hygroscopic growth factor distributions are measured with a scan time of 90 s. Hygroscopic growth measurements for a given dry particle diameter are repeated and the particle counts arrays summed until a prescribed minimum number of particles are counted. The HTDMA went through an automated calibration each night shortly after midnight. That, coupled with time taken for some additional types of measurements not used here, results in the reduced measurement frequency in the early morning that is evident in Figs. 4, 5, and 13.

METHODOLOGY

Growth factor distributions recorded from 2009 to 2012 were used in the analysis. Histograms of mean GF at 90% RH over the 4-year period for 13, 25, 50, 100, 200, and 400 nm dry diameter particles are presented in Fig. S2. The measured distributions were first used to calculate hygroscopicity parameter (*kappa* or κ) distributions for all six particle sizes using κ-Köhler theory (Petters and Kreidenweis, 2007).

$$\kappa = (GF^3 - 1)\left(\frac{\exp\left(\frac{4M_w(\sigma_s / a)}{RT\rho_w D}\right)}{RH} - 1\right) \quad (1)$$

where M_w is the molecular weight of water, $\sigma_{s/a}$ the surface tension at the solution and air interface, R the universal gas constant, T the temperature, ρ_w the density of water, and D the aqueous particle diameter at a given RH. Averages of κ were calculated for three different time spans of the day: morning (midnight–10:30 am), day (10:30 am–7:00 pm), and night (7:00 pm–midnight). Further, separate morning, day, and night averages of κ were calculated for days with and for days without NPF events for which the particle mode grew past 13 nm (referred to simply as NPF event days later).

The analysis here largely focuses on the dominant GF mode/modes at the six particle sizes for which GF distributions are routinely measured. Each mode was fitted and then categorized into one of three hygroscopicity groups: hygroscopic ($GF > 1.3$), less-hygroscopic ($1.3 \geq GF > 1.15$), and nearly-hydrophobic ($GF \leq 1.15$). Different particle types within an external mixture generally have different hygroscopicity, resulting in GF distributions with a single broad mode or multiple narrow modes, and correspondingly high *SD*. In contrast, all particles in internal aerosol mixtures have the same composition and, therefore, the same hygroscopicity, leading to unimodal and narrow GF distributions with low *SD*. Here, the *SD* of the GF distributions is used to quantify the aerosol (hygroscopicity) mixing state, similar to the approach of Holmgren *et al*. (2014). Specifically, we use the ratio of the GF distribution *SD* calculated for each measurement, $SD_{measurement}$, to a reference value, $SD_{int/ext}$, that is selected to roughly represent the separation between a more internal and a more external

mixture at that size. That reference value is based on the lowest *SD* values observed over the 4-year period, which are assumed to represent the values for an internal mixture. Fig. 2 presents the calculated *SD* for every GF distribution measured from 2009 to 2012.

The rightward extension and the increased breadth of the histograms in Fig. 2 for the smaller and the larger particles is due partially to the increased frequency of broad and/or multi-modal GF distributions and to greater compositional variability over time, respectively. But size-dependent characteristics of the HTDMA response also contribute. The breadth of the GF distributions for the smaller particles (e.g., 13 nm) is increased due to diffusional broadening (Stolzenburg, 1988). For measurements of the larger particles (e.g., 400 nm) the instrument flow rates are automatically reduced, which broadens the instrument response due to an increased impact of mixing (or smearing) in the tubing connecting the condensation particle counter (CPC) to the downstream DMA outlet (Russell *et al*., 1995; Collins *et al*., 2002). The GF distributions for the small and large particle size tails of the size range also tend to be noisier due to low particle counts, and are therefore more sensitive to false counts. Thus, because the *SD* of a true internally mixed aerosol would vary with particle size, the reference value used for the mixing state quantification is also assumed to be size-dependent. Somewhat arbitrarily, the reference *SD* for each dry size is defined based on that corresponding to the 10% cumulative frequency, $SD_{10\%}$, for all observations, which is shown in Fig. 3 as the intersection of each of the cumulative frequency curves with the dashed horizontal line. Based on visual inspection of the results for different GF distributions, $SD_{int/ext}$ was defined as $1.4 \times SD_{10\%}$, with the results for all sizes also shown in Fig. 3. For each measurement, a hygroscopicity-based mixing state value was calculated as $MS_{hyg} = SD_{measurement}/SD_{int/ext}$. A GF distribution with an MS_{hyg} higher (lower) than 1 indicates a more external (internal) mixture for that particle size.

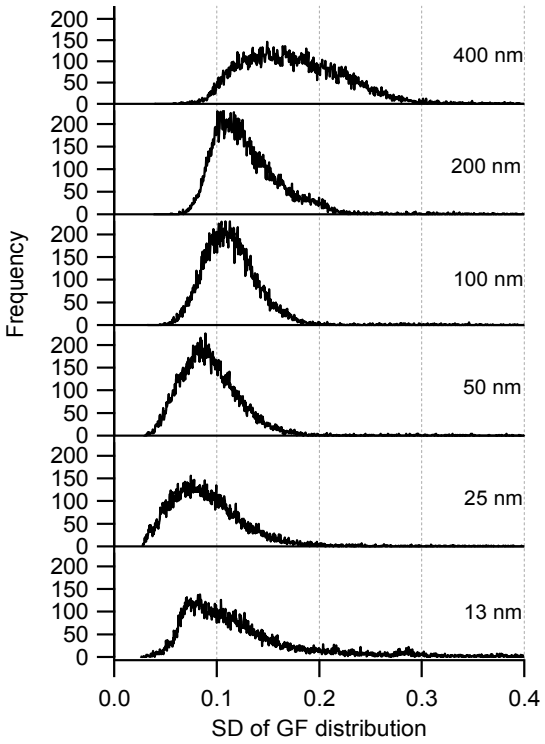

Fig. 2. SD histograms for all GF data from 2009 to 2012.

RESULTS AND DISCUSSION

Diel Variation in Kappa (κ)

The hygroscopicity parameter, *κ*, was determined for each mode in all GF distributions measured over the 4-year period. Among the commonly observed aerosol hygroscopicity characteristics at the site is the diel pattern evident in the example 4-day time series shown in Fig. 4. For all particle sizes, *κ* is generally higher during the day than at night. A similar result is obtained when hourly *κ* is averaged over the full 4-year period (Fig. 5), which is consistent with observations reported by Ehn *et al.* (2007) and Liu *et al.* (2011). For all sizes the maximum *κ* is observed around 3 pm. Generally, particles smaller than 100 nm are least hygroscopic in the morning around 5–6 am, while larger particles are so around midnight. The daytime enhancement in hygroscopicity likely accompanies production of soluble secondary inorganic and organic species through reactions with hydroxyl radical, OH·, and ozone, O_3, both of which are most concentrated during the day. Nocturnal atmospheric inversions and enhanced partitioning of some less

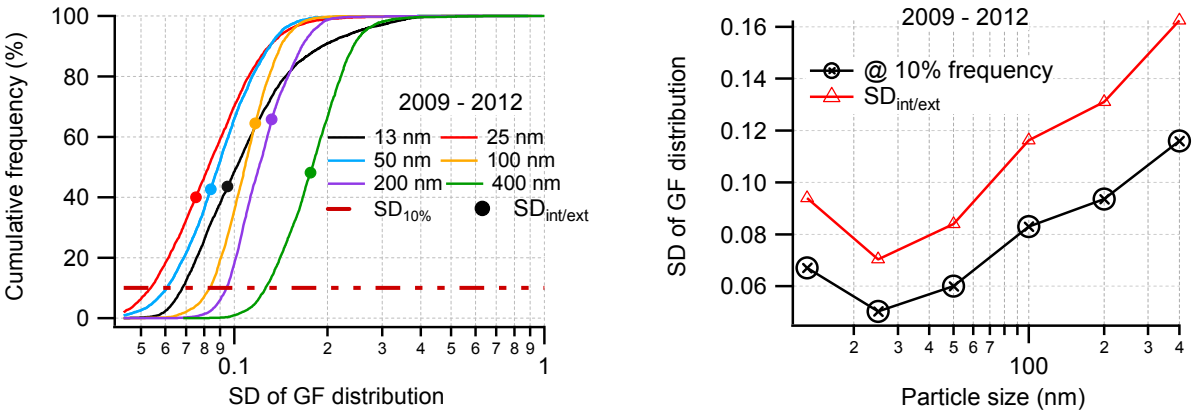

Fig. 3. Cumulative frequency vs. SD (left) and SD at 10% cumulative frequency and $SD_{int/ext}$ (right).

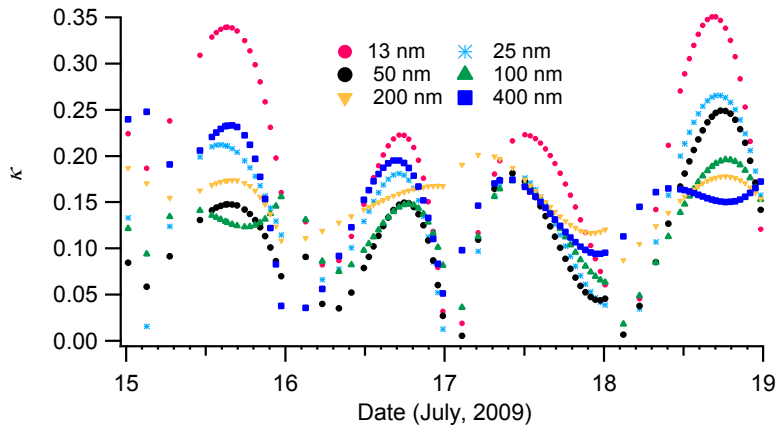

Fig. 4. Diel variation in κ from 15 to 18 July, 2009.

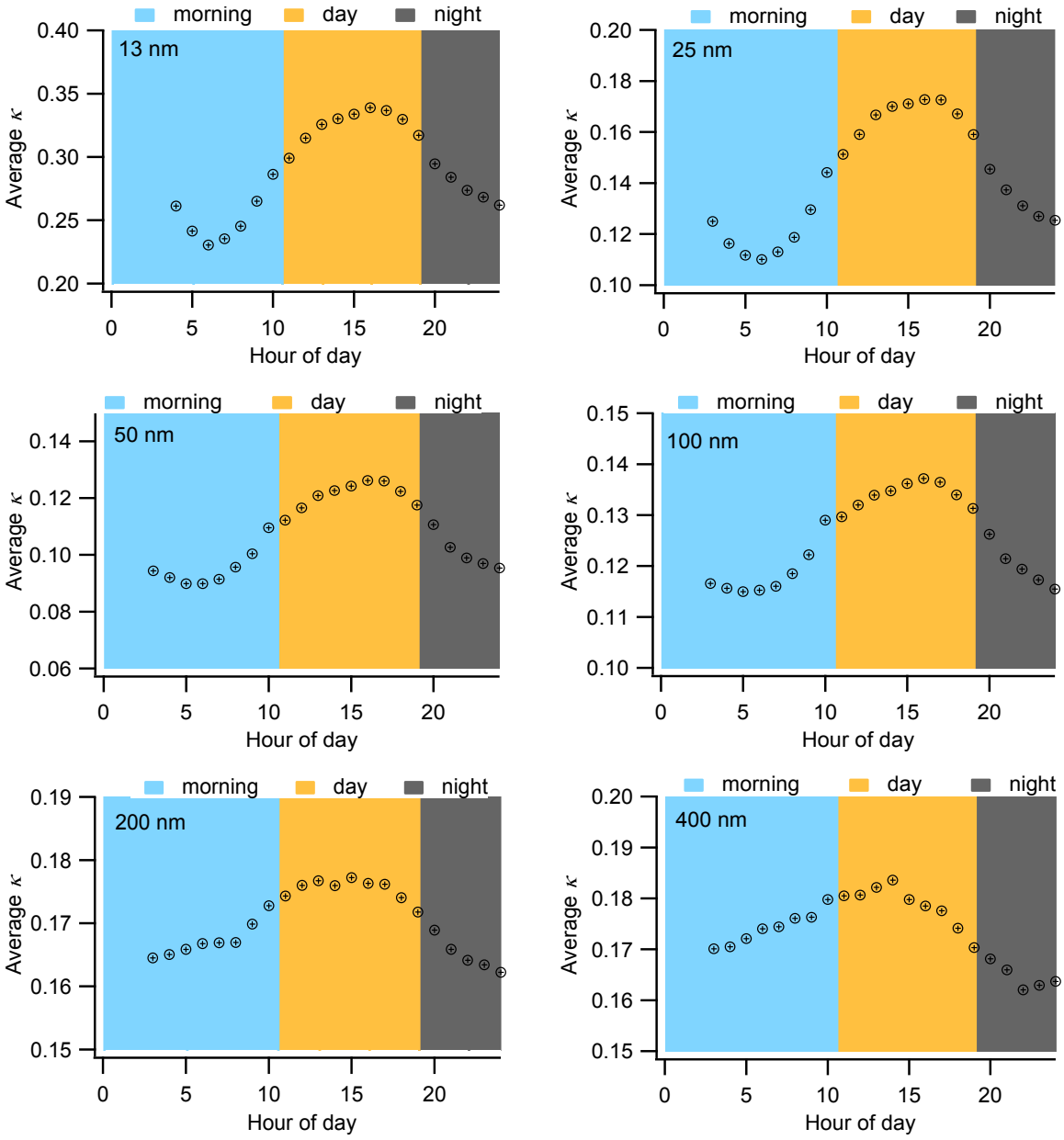

Fig 5. Diel variation in hourly κ averaged over 2009–2012. Blue, yellow, and gray correspond to the time spans of morning, day, and night defined in the text.

hygroscopic organics into the aerosol phase (Sellegri *et al*., 2005) can lower the nighttime hygroscopicity as well. Annual averages of morning, day, and nighttime κ as a function of particle size are presented in Fig. 6, which displays a diel pattern similar to that shown in Figs. 4 and 5. Because the relative change in mass due to condensation is greatest for small particles, the diel variations are also more pronounced with them.

Seasonal Variation in Kappa (κ)

Seasonal variation in the daily-averaged κ for the 4-year period is shown in Fig. 7. The seasonal peaks/depressions in aerosol hygroscopicity are categorized as winter peaks (observed in 200 nm and 400 nm data), spring peaks (13–100 nm), summer peaks (13–100 nm and 400 nm), autumn peaks (13–100 nm), and autumn depressions (200 and 400 nm). The spring, summer and autumn peaks are seen for the 13–100 nm data. Spring and summer peaks correspond to increased biogenic emissions, photochemical activity, and periodic fertilizer application for crops such as corn, canola and soybean. Also, the southerly winds that are dominant during this period often carry hygroscopic anthropogenic species such as sulfate. The lower amplitude peaks in autumn for particles smaller than 100 nm may result from fertilizer application before planting of winter wheat. Increased concentrations of dust and organic soil particles from crop harvesting contribute to the depression in hygroscopicity of larger particles in autumn, while planting of several types of crops and typically higher wind speeds in the spring contribute to the observed depression in 400 nm particle hygroscopicity. The increased hygroscopicity of 200 nm and 400 nm particles in the winter is probably associated with increased nitrate formation at low temperature.

Size Dependence of κ

Fig. 6 presents the variation of κ with size and time of day. It is evident from the figure that κ has a strong size dependence. Averaged over the year, very small particles are more hygroscopic, perhaps due to a higher content of more hygroscopic species such as sulfate and organic salts that have sufficiently low volatility to condense despite the large particle curvature. Hygroscopicity then tends to gradually decrease with increasing size. Though no direct evidence of the cause of this pattern is available, it can be explained by growth in this size range that results from condensation of less-hygroscopic organic species. This trend reverses for particles larger than 50 nm, which are likely cloud active and may have grown through aqueous phase formation of sulfate and oxygenated organics. Wang *et al*. (2007) showed that aqueous phase production had a discernable impact on the aerosol measured from an aircraft in the vicinity of SGP. Within the measured size range, 50 nm particles have the lowest average κ. The small particle (left side) tail of the coarse dust mode often impacts the 600 nm GF distributions, which results in a time dependent variation that is not closely connected with that of the smaller particles. Thus, only the results for the 13 to 400 nm sizes are presented here.

NPF Event vs. Non-Event Day κ

The monthly frequency of NPF events during 2009 is presented in Fig. 8. The frequency increased around the beginning of spring and remained high through the summer. This likely reflects heightened photochemical activity and increased biogenic emissions over this time. Particle formation was rarely observed in the winter during that year. All NPF events were identified visually following the criteria described by Dal Maso *et al.* (2005): i) Within the size distribution a distinct new mode should appear, ii) the mode should be within the nucleation size range (< 25 nm), iii) the mode should be present for several hours (3 h in our study), and iv) the mode should grow. The timing of

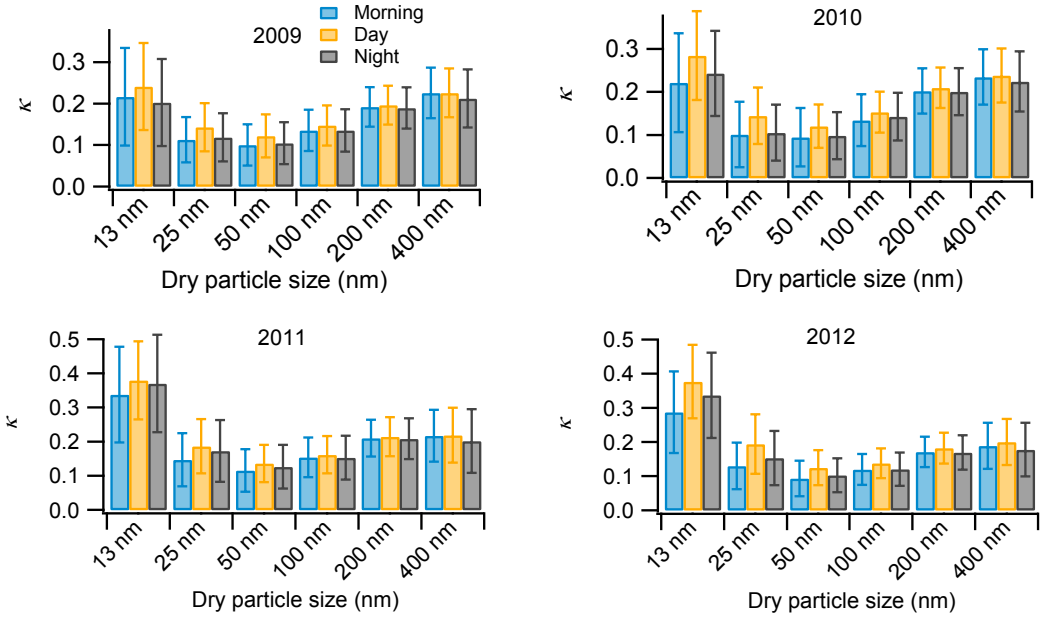

Fig. 6. Annually averaged κ for morning, day, and night for each of the four years. Time is in CST.

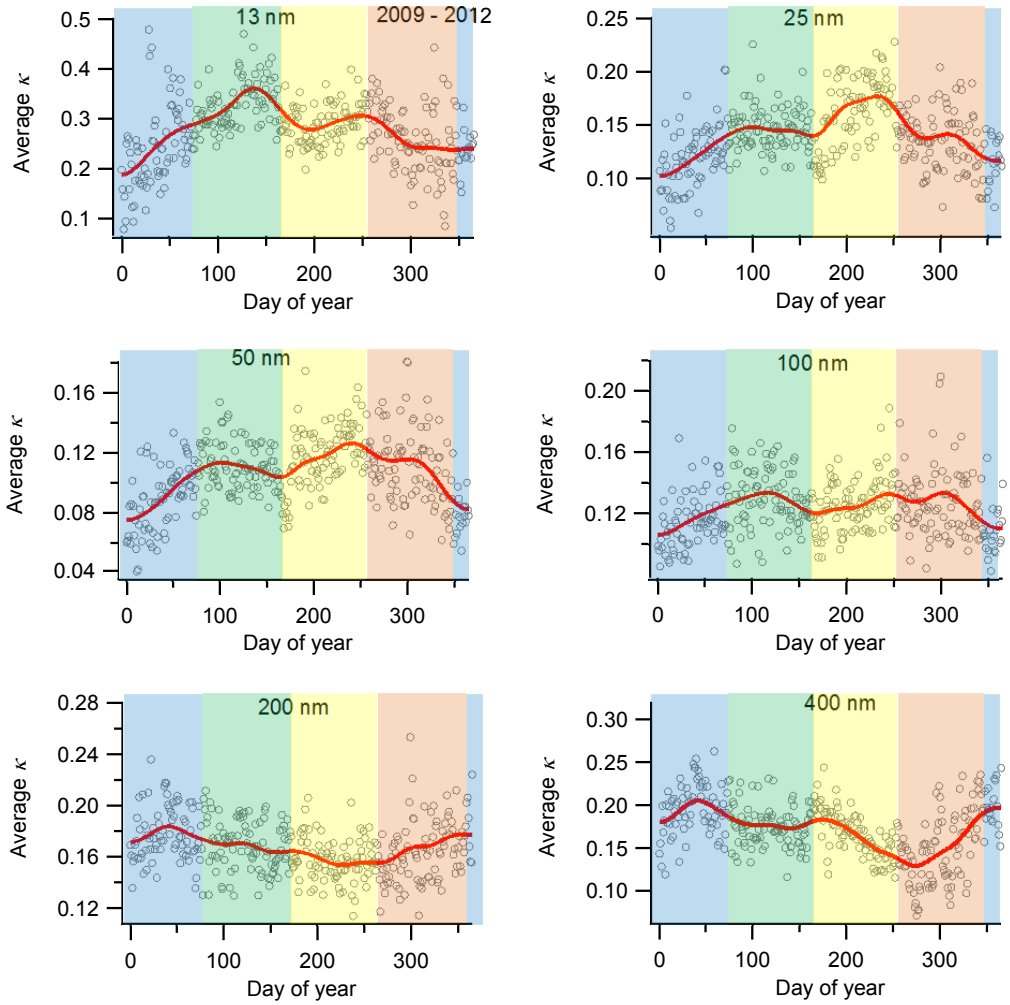

Fig. 7. Seasonal variation in daily κ averaged over 2009–2012. Blue, green, yellow and orange correspond to winter, spring, summer, and autumn, respectively.

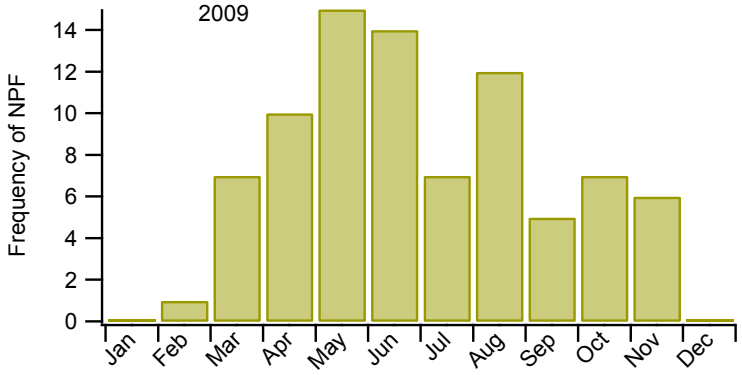

Fig. 8. Monthly frequency of NPF in 2009.

the initial detection of the nucleation mode as it reached the lower limit of the measurement size range (i.e., 12 nm) is shown in Fig. 9 for the same time period. Although it varies widely due to its dependence on meteorological parameters, new particles were most frequently detected between noon and 2 pm. The difference in hygroscopicity between days with and days without NPF events is presented in Fig. 10 as the ratio of respective κ of the 6 particle sizes.

The κ of smaller particles was usually higher on NPF event days than on non-event days, especially during the daytime. This in part reflects production of more hygroscopic condensable species on days on which there is active photochemistry and, consequently, an increased likelihood of NPF. This hygroscopicity enhancement on

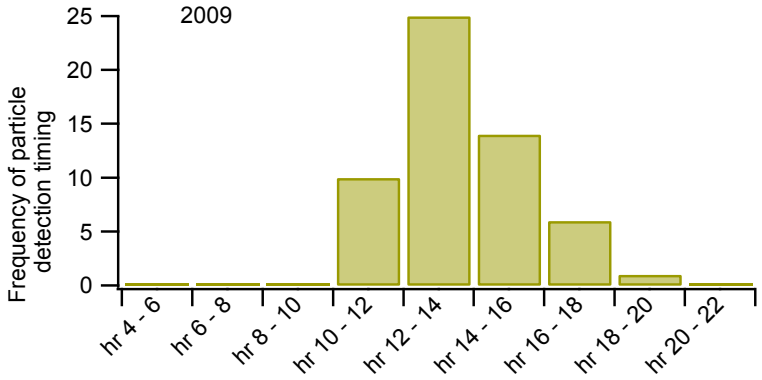

Fig. 9. Frequency of nucleation mode particle detection time on NPF event days in 2009. Time is in CST.

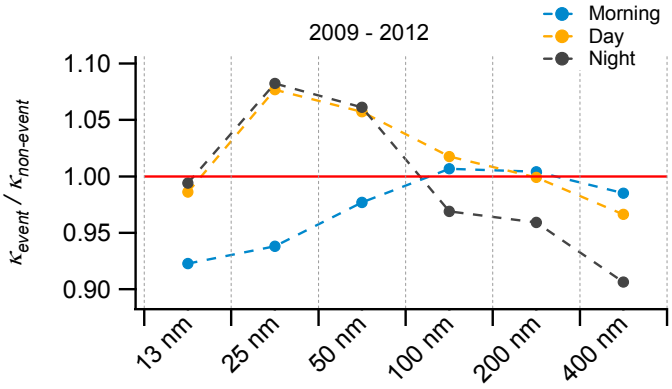

Fig. 10. Average NPF event day κ to non-event day κ ratio for all measurements from 2009–2012. Markers above (below) the red line indicate higher (lower) κ on NPF event days than on non-event days.

NPF event days is not evident for the 200 and 400 nm particles. This is not unexpected as the NPF mode does not grow into that size range in a day and so any connection between κ of those large particles and the events comes from the common influence of the meteorological and chemical conditions that favor NPF. The average morning time κ of smaller particles (13–50 nm) on NPF event days is lower than that on non-event days. According to Ehn *et al*. (2007), NPF event days at Hyytiälä are similarly often preceded by a significant concentration of less hygroscopic aerosols, which lowers the morning-time average κ. A plausible explanation for this relationship is that lower morning time hygroscopicity results in lower hydrated aerosol surface area concentration and condensation sink, thereby reducing competition for low volatility species that contribute to nucleation and small particle growth. However, that connection was not found to be significant in these data. Thus, the responsible mechanism or reason for association is not evident from the analyzed data. The relative changes in κ at different times of day (i.e., morning, day, night) and types of day (i.e., NPF event, non-event) are summarized in Fig. 11. The result that all points lie above the red line indicates that the hygroscopicity is highest during daytime for all sizes. Usually the increase in κ from morning to daytime is higher than the decrease in κ from daytime to nighttime for particles smaller than 100 nm. This change is greatest for 25 nm particles during NPF event days. The reverse trend is evident in particles larger than 100 nm. For example, the average NPF event daytime κ of 25 nm particles was 1.5 times higher than that in the morning and 1.2 times higher than that at night, whereas for 400 nm particles the average κ during the daytime was similar to that in the morning and 1.13 times higher than that at night. Thus, the hygroscopicity of smaller particles is higher at night than in the morning, while for larger particles it is slightly higher in the morning than at night.

Mode Resolved Hygroscopicity

As described in the methodology section, modes of GF distributions were classified into three groups. The relative occurrence frequencies at each size and for each year are shown in Fig. 12. A majority of the modes in the GF distributions for particles within the 25–100 nm size range were classified as either less-hygroscopic or nearly-hydrophobic. But at larger sizes (> 100 nm) there were higher concentrations of hygroscopic and nearly-hydrophobic particles. At least averaged over each year, nearly-hydrophobic particles, which includes fresh carbonaceous aerosols and dust (at larger sizes), are present across the entire size range. Water soluble organic species likely make up a significant fraction of the < 100 nm particles in the less-hygroscopic category. Increasing sulfate content in cloud active particles and increasing nitrate content in those particles onto which volatile ammonium nitrate efficiently

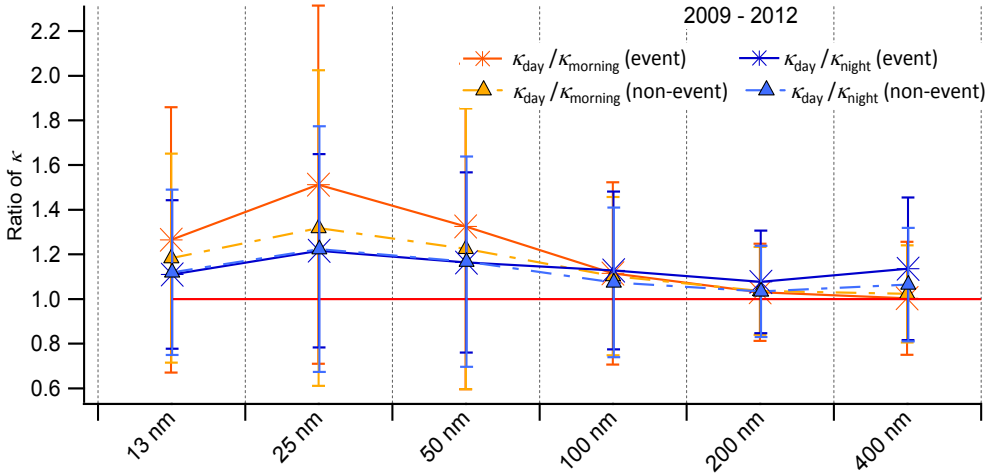

Fig. 11. Change in κ from morning to day (orange) and day to night (blue) averaged on NPF event days (star), and non-event days (triangle) from 2009–2012.

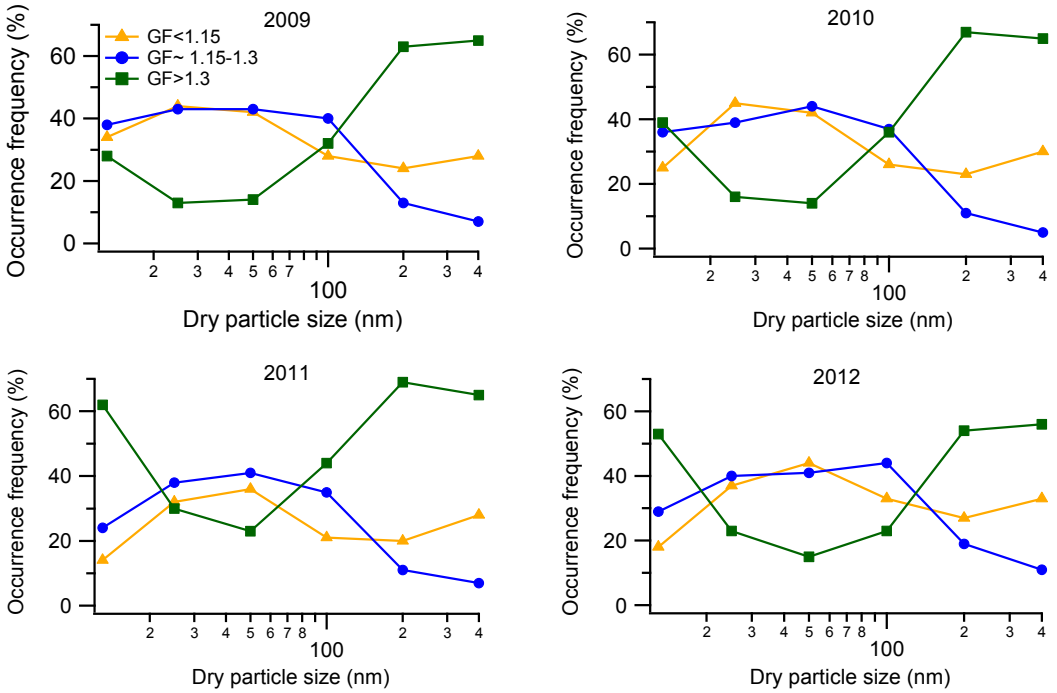

Fig. 12. Occurrence frequency of GF modes in three hygroscopicity groups for each of the four years.

condenses contributes to the increased frequency of hygroscopic modes for the larger particles. Similar variations with particle size were observed by Gasparini *et al*. (2006), Levin *et al*. (2014), and Swietlicki *et al*. (2008).

Quantifying Mixing State: Diel Variation

The SD ratio at each particle size was used to quantify aerosol mixing state as described in the methodology section. An example time series for 14–18 June, 2009 is shown in Fig. 13. As is true for this 5-day period, a diel pattern is typically observed. The greater frequency of MS_{hyg} below the 'MS_{hyg} = 1' line during the daytime in Fig. 13 indicates more frequent internal mixtures, which is likely the result of condensational growth.

Quantifying Mixing State: Seasonal Variation

The daily average MS_{hyg} is plotted in Fig. 14 for all measurements made between 2009 and 2012 to illustrate seasonal variation. The relatively lower MS_{hyg} during summer months across all sizes is suggestive of more internally mixed aerosols at that time of the year. This pattern may partially reflect seasonality in air mass origin as southerly winds are more common during the warmer months and precursor emissions are generally higher south of SGP. Higher biogenic emissions, temperature, and UV intensity during the warmer months also promotes condensational growth that contributes to formation of internally mixed aerosols. In contrast, in the winter enhanced emission of fresh carbonaceous aerosol Parworth *et al.* (2015), lower temperatures, and shorter

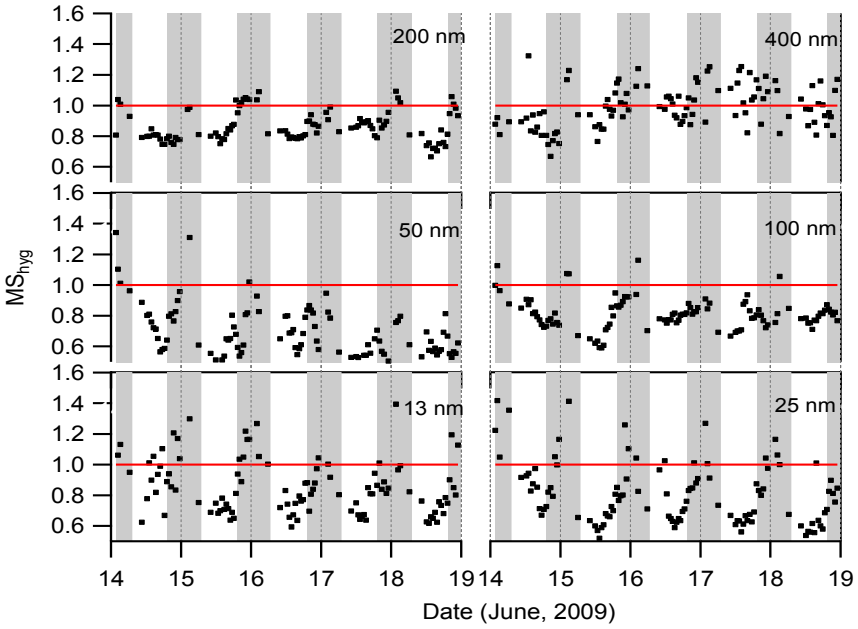

Fig. 13. Diel pattern in hygroscopicity based mixing state from 14 to 18 June, 2009. The light gray shading bands represent nighttime. Time is in CST.

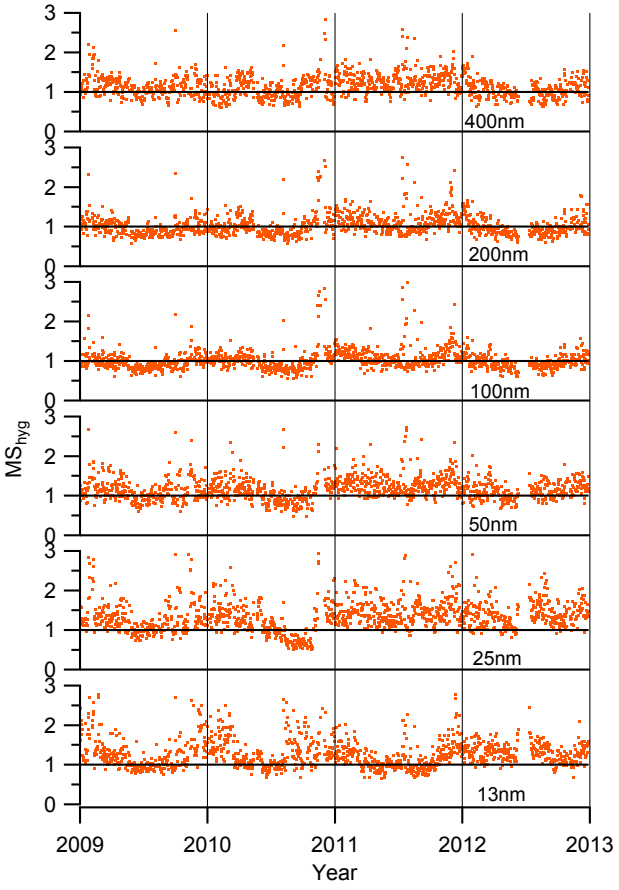

Fig. 14. Annual pattern in daily average MS_{hyg}.

daylight period result in an increased frequency of external mixtures. Holmgren *et al.* (2014) observed a similar seasonal trend in aerosol mixing state at Puy de Dôme, France.

SUMMARY

Hygroscopic growth factor distributions measured between 2009 and 2012 at the DOE Southern Great Plains (SGP) site were used to calculate size- and time-dependent hygroscopicity parameters (κ), which were then averaged over different time periods. The average κ was highest during the day regardless of particle size, likely due to increased photochemical production of soluble secondary inorganic and organic species. This trend was more apparent in smaller particles as their relative change in mass from condensation is greater. For each of the 4 years, 50 nm particles were least hygroscopic on average, with hygroscopicity monotonically increasing with increasing size for larger particles and with decreasing size for smaller particles. Averaged daytime κ on days with NPF events were higher than on days without events for measurements at dry diameter less than 200 nm that are more directly influenced by the growing mode of nucleated particles.

Modes present in the GF distributions were categorized into three hygroscopicity groups (hygroscopic, less-hygroscopic, and nearly-hydrophobic). At all sizes, modes categorized as nearly-hydrophobic were frequently observed, reflecting the presence of primary carbonaceous particles and/or dust. Consistent with the size-dependent variation in average κ, modes classified as hygroscopic were more frequently observed at the small and large particle tails of the size range. A diel pattern was observed in the hygroscopicity-based mixing state, MS_{hyg}, which is defined as the ratio of the calculated SD for a measured GF distribution and a size specific threshold SD roughly separating internal and external mixing states. Values were lower during the day than at night and during the summer than during the winter, reflecting more internal mixing during periods of enhanced photochemistry that likely results from

uniform condensational growth and photochemical aging.

ACKNOWLEDGMENTS

We acknowledge funding from U.S. Department of Energy as part of the Atmospheric Radiation Measurement Program. All data used in our analysis were downloaded from the DOE ARM data archive at http://www.archive.arm.gov/. Derived products in the manuscript can be obtained by contacting Dr. Don Collins (dcollins@tamu.edu).

SUPPLEMENTARY MATERIAL

Supplementary data associated with this article can be found in the online version at http://www.aaqr.org.

REFERENCES

Abbatt, J., Broekhuizen, K. and Pradeepkumar, P. (2005). Cloud condensation nucleus activity of internally mixed ammonium sulfate/organic acid aerosol particles. *Atmos. Environ.* 39: 4767–4778.

Choi, M.Y. and Chan, C.K. (2002). The effects of organic species on the hygroscopic behaviors of inorganic aerosols. *Environ. Sci. Technol.* 36: 2422–2428.

Collins, D.R., Flagan, R.C. and Seinfeld, J.H. (2002). Improved inversion of scanning DMA data. *Aerosol Sci. Technol.* 36: 1–9.

Collins, D.R. (2010). Tandem Differential Mobility Analyzer/ Aerodynamic Particle Sizer (APS) Handbook. DOE/SC-ARM-TR-090. https://www.arm.gov/publications/tech_reports/handbooks/tdma_handbook.pdf.

Cruz, C.N. and Pandis, S.N. (2000). Deliquescence and hygroscopic growth of mixed inorganic-organic atmospheric aerosol. *Environ. Sci. Technol.* 34: 4313–4319.

Dal Maso, M., Kulmala, M., Riipinen, I., Wagner, R., Hussein, T., Aalto, P.P. and Lehtinen, K.E.J. (2005). Formation and growth of fresh atmospheric aerosols: Eight years of aerosol size distribution data from SMEAR II, Hyytiälä, Finland. *Boreal Environ. Res.* 10: 323–336.

Dick, W.D., Saxena, P. and Mcmurry, P H. (2000). Estimation of water uptake by organic compounds in submicron aerosols measured during the Southeastern Aerosol and Visibility Study. *J. Geophys. Res.* 105: 1471–1479.

Duplissy, J., Gysel, M., Alfarra, M.R., Dommen, J., Metzger, A., Prevot, A.S.H., Weingartner, E., Laaksonen, A., Raatikainen, T., Good, N., Turner, S.F., Mcfiggans, G. and Baltensperger, U. (2008). Cloud forming potential of secondary organic aerosol under near atmospheric conditions. *Geophys. Res. Lett.* 35: L03818.

Ehn, M., Petäjä, T., Aufmhoff, H., Aalto, P., Hämeri, K., Arnold, F., Laaksonen, A. and Kulmala, M. (2007). Hygroscopic properties of ultrafine aerosol particles in the boreal forest: Diurnal variation, solubility and the influence of sulfuric acid. *Atmos. Chem. Phys.* 7: 211–222.

Fiedler, V., Maso, M.D., Boy, M., Aufmhoff, H., Hoffmann, J., Schuck, T., Birmili, W., Hanke, M., Uecker, J., Arnold, F. and Kulmala, M. (2005). The contribution of sulphuric acid to atmospheric particle formation and growth: A comparison between boundary layers in Northern and Central Europe. *Atmos. Chem. Phys.* 5: 1773–1785.

Gasparini, R., Li, R., Collins, D.R., Ferrare, R.A. and Brackett, V.G. (2006). Application of aerosol hygroscopicity measured at the Atmospheric Radiation Measurement Program's Southern Great Plains site to examine composition and evolution. *J. Geophys. Res.* 111: D05S12.

Gunthe, S.S., King, S.M., Rose, D., Chen, Q., Roldin, P., Farmer, D.K., Jimenez, J.L., Artaxo, P., Andreae, M.O., Martin, S.T. and Pöschl, U. (2009). Cloud condensation nuclei in pristine tropical rainforest air of Amazonia: Size-resolved measurements and modeling of atmospheric aerosol composition and CCN activity. *Atmos. Chem. Phys.* 9: 7551–7575.

Gysel, M., Crosier, J., Topping, D.O., Whitehead, J.D., Bower, K.N., Cubison, M.J., Williams, P.I., Flynn, M.J., Mcfiggans, G.B. and Coe, H. (2007). Closure study between chemical composition and hygroscopic growth of aerosol particles during TORCH2. *Atmos. Chem. Phys.* 7: 6131–6144.

Hersey, S.P., Sorooshian, A., Murphy, S.M., Flagan, R.C. and Seinfeld, J.H. (2009). Aerosol hygroscopicity in the marine atmosphere: A closure study using high-time-resolution, multiple-RH DASH-SP and size-resolved C-ToF-AMS data. *Atmos. Chem. Phys.* 9: 2543–2554.

Hodshire, A.L., Lawler, M.J., Zhao, J., Ortega, J., Jen, C., Yli-Juuti, T., Brewer, J.F., Kodros, J.K., Barsanti, K. C., Hanson, D. R., Mcmurry, P. H., Smith, J. N. and Pierce, J. R. (2016). Multiple new-particle growth pathways observed at the US DOE Southern Great Plains field site. *Atmos. Chem. Phys.* 16: 9321–9348.

Holmgren, H., Sellegri, K., Hervo, M., Rose, C., Freney, E., Villani, P. and Laj, P. (2014). Hygroscopic properties and mixing state of aerosol measured at the high-altitude site Puy de Dôme (1465 m a.s.l.), France. *Atmos. Chem. Phys.* 14: 9537–9554.

Jing, B., Tong, S., Liu, Q., Li, K., Wang, W., Zhang, Y. and Ge, M. (2016). Hygroscopic behavior of multicomponent organic aerosols and their internal mixtures with ammonium sulfate. *Atmos. Chem. Phys.* 16: 4101–4118.

Jurányi, Z., Gysel, M., Duplissy, J., Weingartner, E., Tritscher, T., Dommen, J., Henning, S., Ziese, M., Kiselev, A., Stratmann, F., George, I. and Baltensperger, U. (2009) Influence of gas-to-particle partitioning on the hygroscopic and droplet activation behaviour of α-pinene secondary organic aerosol. *Phys. Chem. Chem. Phys.* 11: 8091.

King, S.M., Rosenoern, T., Shilling, J.E., Chen, Q., Wang, Z., Biskos, G., Mckinney, K.A., Pöschl, U. and Martin, S.T. (2010) Cloud droplet activation of mixed organic-sulfate particles produced by the photooxidation of isoprene. *Atmos. Chem. Phys.* 10: 3953–3964.

Levin, E.J.T., Prenni, A.J., Palm, B.B., Day, D.A., Campuzano-Jost, P., Winkler, P.M., Kreidenweis, S.M., Demott, P.J., Jimenez, J.L. and Smith, J.N. (2014). Size-

resolved aerosol composition and its link to hygroscopicity at a forested site in Colorado. *Atmos. Chem. Phys.* 14: 2657–2667.

Liu, B., Pui, D., Whitby, K., Kittelson, D., Kousaka, Y. and Mckenzie, R. (1978). The aerosol mobility chromatograph: A new detector for sulfuric acid aerosols. *Atmos. Environ.* 1: 99–104.

Liu, P.F., Zhao, C.S., Göbel, T., Hallbauer, E., Nowak, A., Ran, L., Xu, W.Y., Deng, Z.Z., Ma, N., Mildenberger, K., Henning, S., Stratmann, F. and Wiedensohler, A. (2011). Hygroscopic properties of aerosol particles at high relative humidity and their diurnal variations in the North China Plain. *Atmos. Chem. Phys.* 11: 3479–3494.

Mcmurry, P.H. and Stolzenburg, M.R. (1989). On the sensitivity of particle size to relative humidity for Los Angeles aerosols. *Atmos. Environ.* 23: 497–507.

Meyer, N.K., Duplissy, J., Gysel, M., Metzger, A., Dommen, J., Weingartner, E., Alfarra, M.R., Prevot, A.S.H., Fletcher, C., Good, N., Mcfiggans, G., Jonsson, Å.M., Hallquist, M., Baltensperger, U. and Ristovski, Z.D. (2009). Analysis of the hygroscopic and volatile properties of ammonium sulphate seeded and unseeded SOA particles. *Atmos. Chem. Phys.* 9: 721–732.

Parworth, C., Fast, J., Mei, F., Shippert, T., Sivaraman, C., Tilp, A., Watson, T. and Zhang, Q. (2015). Long-term measurements of submicrometer aerosol chemistry at the Southern Great Plains (SGP) using an Aerosol Chemical Speciation Monitor (ACSM). *Atmos. Environ.* 106: 43–55.

Peng, C., Jing, B., Guo, Y.C., Zhang, Y.H. and Ge, M.F. (2016). Hygroscopic Behavior of Multicomponent Aerosols Involving NaCl and Dicarboxylic Acids. *J. Phys. Chem. A* 120: 1029–1038.

Petters, M.D. and Kreidenweis, S.M. (2007). A single parameter representation of hygroscopic growth and cloud condensation nucleus activity. *Atmos. Chem. Phys.* 7: 1961–1971.

Prenni, A.J., Petters, M.D., Kreidenweis, S.M., Demott, P.J. and Ziemann, P.J. (2007). Cloud droplet activation of secondary organic aerosol. *J. Geophys. Res.* 112: D10223.

Russell, L.M., Flagan, R.C. and Seinfeld, J.H. (1995). Asymmetric instrument response resulting from mixing effects in accelerated DMA-CPC measurements. *Aerosol Sci. Technol.* 23: 491–509.

Sellegri, K., Umann, B., Hanke, M. and Arnold, F. (2005). Deployment of a ground-based CIMS apparatus for the detection of organic gases in the boreal forest during the QUEST campaign. *Atmos. Chem. Phys.* 5: 357–372.

Stolzenburg, M., Kreisberg, N. and Hering, S. (1998). Atmospheric size distributions measured by differential mobility optical particle size spectrometry. *Aerosol Sci. Technol.* 29: 402–418.

Stolzenburg, M.R. (1988). An Ultrafine Aerosol Size Distribution Measuring System. PhD Thesis Minneapolis, MN: University of Minnesota.

Svenningsson, B., Rissler, J., Swietlicki, E., Mircea, M., Bilde, M., Facchini, M.C., Decesari, S., Fuzzi, S., Zhou, J., Mønster, J. and Rosenørn, T. (2006). Hygroscopic growth and critical supersaturations for mixed aerosol particles of inorganic and organic compounds of atmospheric relevance. *Atmos. Chem. Phys.* 6: 1937–1952.

Swietlicki, E., Hansson, H.C., Hämeri, K., Svenningsson, B., Massling, A., Mcfiggans, G., Mcmurry, P.H., Petäjä, T., Tunved, P., Gysel, M., Topping, D., Weingartner, E., Baltensperger, U., Rissler, J., Wiedensohler, A. and Kulmala, M. (2008). Hygroscopic properties of submicrometer atmospheric aerosol particles measured with H-TDMA instruments in various environments—a review. *Tellus Ser. B.* 60: 432–469.

Wang, J., Daun, P.H., Kleinman, L.I., Lee, Y., Schwartz, S.E., Springston, S.R., Jonsson, H., Covert, D. and Elleman, R. (2007). Observation of ambient aerosol particle growth due to in-cloud processes within boundary layers. *J. Geophys. Res.* 112: D14207.

Yli-Juuti, T., Nieminen, T., Hirsikko, A., Aalto, P.P., Asmi, E., Hõrrak, U., Manninen, H.E., Patokoski, J., Maso, M.D., Petäjä, T., Rinne, J., Kulmala, M. and Riipinen, I. (2011). Growth rates of nucleation mode particles in Hyytiälä during 2003−2009: Variation with particle size, season, data analysis method and ambient conditions. *Atmos. Chem. Phys.* 11: 12865–12886.

Zhang, X., Mcmurray, P., Hering, S. and Casuccio, G. (1993). Mixing characteristics and water content of submicron aerosols measured in Los Angeles and at the grand canyon. *Atmos. Environ.* 27: 1593–1607.

Received for review, October 13, 2016
Revised, March 21, 2017
Accepted, March 21, 2017